

Optimized multi-coil wireless power transfer for experimental neuroscience settings with live animals: a robust design methodology

Hadi Hayati¹, Guillaume Bilodeau¹, Louison Brochoire^{2,3}, Gabriel Gagnon-Turcotte¹, Pascal Fossat², Yves De Koninck³ and Benoit Gosselin^{1,3,*}

¹Department of Electrical and Computer Engineering, Université Laval, Quebec, Canada

²University of Bordeaux, CNRS, IMN, UMR 5293, F-33000, Bordeaux, France

³CERVO Brain Research Centre, Québec Mental Health Institute, Quebec, Canada

* Correspondence author; E-mail: benoit.gosselin@gel.ulaval.ca.

Abstract: Electrophysiological recording and neural stimulation in freely moving laboratory mice offer significant potential for advancing in neuroscience research, enabling the study of neural activities and brain functions in natural surroundings. Using wireless technologies and miniaturized devices, researchers can monitor and manipulate the electrical activity of neurons in real time while the animals engage in complex behaviors. However, depending on its size and weight, the autonomy of a wireless system is limited to a few minutes or a few hours at most. To address this, a wireless link for continuous power transmission is essential to run practical experiments. Working with mice is challenging due to their small size and limited volume available, necessitating the use of very small coils. It is also crucial to maintain the Specific Absorption Rate (SAR) within safe limits to prevent heating and temperature rises that could interfere with physiological conditions and measurements. This paper introduces a methodology to design an optimized overlapping multi-coil array integrated within a standard home cage, featuring a high-quality factor design that effectively couples with a small, lightweight receiver coil for *in-vivo* measurements with laboratory mice. Using trace adjustment, the transmitter design enhances the self-resonance frequency (SRF) of the coils, resulting in an improved quality factor, with measurements indicating a value of 173 at 6.78 MHz. Using a 0.46-gram, 14-mm receiver (RX) coil, the measurement results reveal a maximum power transfer efficiency (PTE) of 7.5% and a maximum power delivered to the load (PDL) of 23.8 dBm (240 mW) at a 4-cm distance. Additionally, continuous *in-vivo* recording sessions demonstrate the delivery of approximately 46 mW on average wirelessly to the battery using a 0.4-gram, 16-mm RX coil installed on the head of a laboratory mouse. The system also prevents thermal effects in mice tissues, with a peak spatial-average SAR (psSAR) of 1.75 W/kg, which is well below the standard regulatory limits.

Keywords: wireless power transfer; electrophysiological recording; inductive coupling; freely moving rodents; power transfer efficiency; S-parameter; quality factor of the coils; self-resonance frequency

1. Introduction

The ability to record electrophysiological data and stimulate neural pathways in freely moving laboratory mice has opened new doors for studying brain function in their natural environments. The integration of wireless technology and compact neuroscience tools now allows scientists to observe and influence neuronal electrical activity in real-time, all while the animals are actively behaving in their usual surroundings [1]. This approach allows for the exploration of neural circuits underlying complex behaviors, such as navigation, social interactions, and learning, without the constraints imposed by tethered systems or anesthesia. Furthermore, neural stimulation can be precisely targeted to modulate specific brain regions or circuits, providing insights into the causal relationships between neural activity and behavior. These techniques are essential for understanding the dynamic nature of brain function and hold promise for developing novel therapeutic strategies for neurological disorders [2,3]. However, due to the stress and restrictions that tethered systems impose on the natural behavior of freely moving animals, the use of a wireless interface for power transfer becomes essential [4]. Additionally, size and weight limitations of the system—attached to the animal—do not allow for generating an energy source that would be sufficient for weeks of monitoring. The goal is to develop wireless and even battery-less neuroscience platforms that are lightweight, minimally invasive, and reduce the risk of infection from percutaneous wire



Copyright©2024 by the authors. Published by ELS Publishing. This work is licensed under a Creative Commons Attribution 4.0 International License, which permits unrestricted use, distribution, and reproduction in any medium provided the original work is properly cited

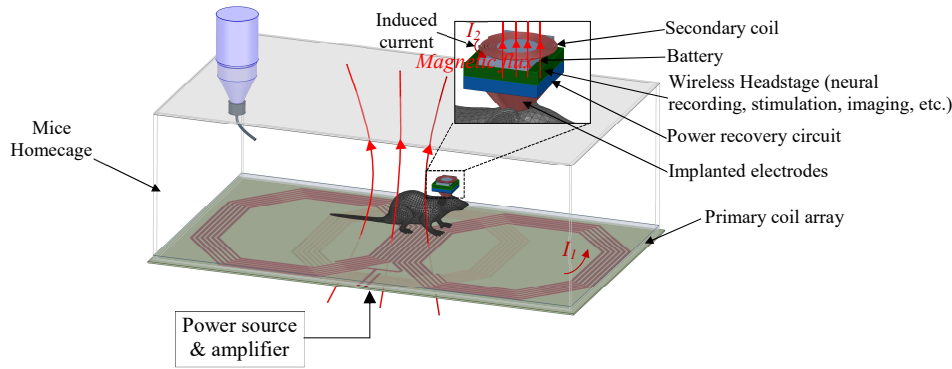


Figure 1. The utilization of inductive-coupling WPT inside a homecage to power up a wireless bioinstrument, like a neuro-recording headstage or a neuro-imaging device, attached or implanted in the body of laboratory mice.

connections or electrolyte leakage from the battery, among other concerns [5]. Considering the amount of energy typically required to power up these platforms (>10 mW), advanced research on new techniques for wireless power transfer (WPT) is essential to ensure sufficient and uninterrupted power delivery, eliminating the need for frequent battery replacements. A power source of tens of milliwatts [6] is typically required for multimodal electrophysiological brain recording and simultaneous multichannel optogenetics stimulation, which involve controlling neural activity using optical systems and genetic engineering technologies during *in-vivo* experiments [7–9]. So far, several solutions have been presented for wireless power transmission including capacitive, ultrasound, and inductive coupling. Capacitive coupling can provide higher power delivered to the load (PDL) compared to the other two methods with better efficiency, but it needs two pairs of large metal pads which pose a challenge for use in miniature devices. Additionally, given the size constraints of metal plates permissible in neuroscience applications, the transmission distance in a capacitive link is limited to a few millimeters [10]. Ultrasound is a viable candidate for providing sufficient power to deep implants; however, its application is limited to areas of the body with soft tissue due to significant attenuation by bone [11]. In contrast, inductive coupling can transmit power over longer distances than capacitive coupling and, unlike ultrasound, can be used in a variety of applications since different organs do not significantly attenuate the signal [11]. Therefore, inductive coupling is a practical solution for providing sufficient power at the desired distance in this application.

Figure 1 illustrates the application of a WPT system in a mice homecage. An inductive WPT link is embedded within the homecage to power up small bioinstruments, such as an electrophysiology recording headstage or neuro-imaging devices, equipped with a power receiver coil attached or implanted in the body of a laboratory mouse. The inductive WPT link includes a power amplifier injecting current into a primary coil where it produces magnetic flux. On the secondary side (the receiver), the flux is induced into another coil that provides current for a headstage. For instance, a wireless headstage equipped with a receiver coil is employed for recording and stimulation of neural activity using electrodes implanted in the brain of a mouse (as shown in the inset of Figure 1). A major concern when designing mm to cm-sized neuroscience platforms is the low coupling coefficient between the receiver (RX) coil and transmitter (TX) coil at distances longer than the diameter of the RX coil. With this configuration, achieving sufficient power delivered to the load through a 2-coil inductive link becomes challenging. To address this issue, a 3-coil architecture using an additional resonator was proposed to power up an implant in [12]. In their work, the TX coil is located above the human head and the resonator coil, along with the mm-sized RX coil, is located on the brain surface.

Figure 2 shows a typical multi-link inductive coupling with resonators between TX and RX coils. Higher number of coupling links with several resonator coils in between have been proposed in [13–15]. In order to have a resonator that can contribute to increasing the power transfer efficiency (PTE), it is optimal for the diameters of L_{r1} and L_{r2} to be larger than the diameter of L_2 . However, this approach can add extra weight due to the resonator coil(s) added on the receiver side, which may burden the mice. Other solution that can result in higher PTE is to increase operating frequency, but specific absorption ratio (SAR) will be degraded at higher frequencies, potentially increasing the temperature and harming the tissues. To overcome this problem, a dual-band WPT system for powering up a mm-sized implant was proposed in [13] that employed two multi-coil inductive links. The first band at 13.56 MHz delivers power through a 4-coil link from the homecage to a wearable wireless interface, and the second band is a 3-coil link that delivers power from the interface to the implant at 60 MHz. This dual-band approach provides enough power to the load with relatively low efficiency, ranging from 0.24% to 0.36%. It should also be noted that there is a second power amplifier (PA) in the wireless interface that delivers power to the implant. This PA consumes a remarkable amount of power that was received by the first link [13].

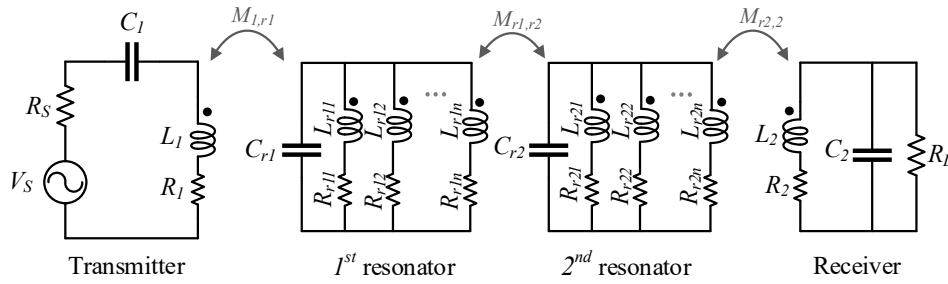


Figure 2. Extended topology of an inductive coupling WPT with resonators.

In [16], a new figure of merit was proposed that gives a higher weight to PDL. Therefore, an operating frequency of tens of MHz was concluded to be the optimal carrier frequency for mm-sized implants.

There have been several works in inductive WPT for small-sized implants that operate at different frequencies, ranging from several MHz to hundreds of MHz. The design in [17] employed a 120-MHz operating frequency to power up an integrated chip with an outer diameter of 1 mm. To implement an inductive link in a homecage where a rodent's behavior can be monitored, several studies have employed arrays of parallel coils. In [18], several identical overlapping coils are connected in parallel to transmit uniform power above a surface suitable for *in-vivo* experiments. The demand for an array of standard homecages, such as the Energized Homecage (EnerCage HC) that can fit into a rack, is growing as researchers study the behaviors of freely moving rodents. The primary challenge with multiple EnerCage-HC setups is cross-coupling between the adjacent homecages, which causes resonance frequency bifurcation. This phenomenon reduces the transmission coefficient of the inductive link, which is worsened by the addition of resonators. In [19], an auto-tuning mechanism was implemented for the problem caused by the bifurcation of seven EnerCage-HC units. In [20] and [21], reactive resonant shielding was introduced to reduce the cross-couplings between nearby homecages. It should be noted that the bifurcation arises from the floating resonators that affect primary and secondary coils' quality factor and transmission coefficient. The resonator coils made of copper foil around the homecage can increase the overall PTE of the link [22], but their large size leads to significant coupling with nearby homecages, complicating tuning and hindering the development of a robust WPT system for animal research. Comparisons between two-coil and three-coil inductive links have shown that the three-coil topology is more advantageous with larger load values and at longer distances [23]. In [24], an experiment on a freely behaving rat was conducted using an array of overlapping planar spiral coils as the driver. The magnetic fields are focused on the location of the rat using several magnetic sensors that track its position and provide 20 mW to the load. However, the wireless interface includes two RX coils that increase the moving part's weight. In [25], two cylinder-type coils were used as the TX power driver with an input of 10 W for brain stimulation of a mouse. A PDL of 0.3 – 1.93 W was obtained, but the size of the RX coil was 35 mm × 20 mm.

In this paper, we present a methodology toward designing an optimized single-link multi-coil inductive coupling WPT system without resonators for a mice homecage. We show that, with a minimal number of overlapping coils on the TX side and a single lightweight coil on the RX side, a reliable WPT is achievable. This approach results in a higher self-resonance frequency (SRF) at the TX, leading to reduced parasitic effects and, consequently, higher efficiency. The presented method enables continuous battery charging during *in-vivo* measurements with mice in a standard homecage during recording sessions. The rest of the paper is organized as follows: Section 2 covers the design challenges associated with the inductive coupling approach. Section 3 outlines the design procedures and presents simulation results using HFSS, while also addressing safety considerations. Experimental results are given in Section 4. *In-vivo* validations and conclusions are presented in Sections 5 and 6, respectively.

2. Design challenges

The main concern over designing a reliable inductive WPT system has always been providing enough PDL, keeping in mind that PTE must be high to limit power losses in the surrounding tissues, which can cause heating effects. In a simple two-coil inductive link of Figure 2 (without resonators), if both primary and secondary loops, L_1C_1 and L_2C_2 , get tuned at the same frequency, then maximum PTE and PDL for this inductive coupling link will be obtained. The maximum PTE of such an inductive link at the optimal load resistance is defined as [26]:

$$\eta_{max} = \frac{k^2 Q_1 Q_2}{(kQ_1 + 1)(kQ_2 + 1)} \quad (1)$$

where ω is the operating frequency, $Q_1 = L_1 \omega / R_1$, $Q_2 = L_2 \omega / R_2$, and R_1 and R_2 are the parasitic resistances of

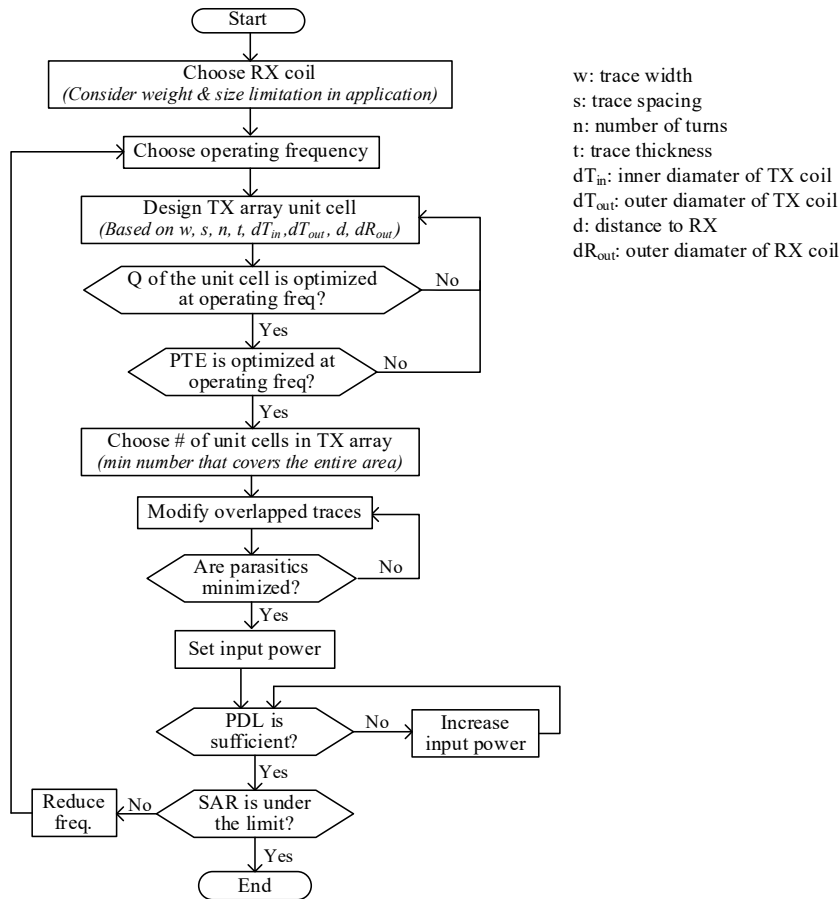


Figure 3. Flowchart of the design procedure.

L_1 and L_2 , respectively. The parameter k is the coupling coefficient between L_1 and L_2 that is mainly defined by the distance between the two of them. As can be seen from (1), PTE is influenced by multiple interrelated parameters. Therefore, an optimum PTE for one configuration of the inductive link does not guarantee the same for another configuration. PTE highly depends on the geometries of TX and RX coils and the distance between them that is reflected in k [27]. The size of the RX coil is typically limited by the application in which the coil will be used. Therefore, to maximize PTE (and PDL accordingly), the diameter of the RX coil should be increased up to the limit, as a small RX coil restricts the choice of frequency. The upper limit of a RX coil's size is determined based on the overall weight of the headstage that mice can carry without trouble. A headstage excluding RX coil and battery can weigh around 1 to 2 grams for mice and up to 5 grams for bigger rodents like rats [28].

To provide sufficient PDL, TX power can also be increased. However, it can only be increased to the point that the exposure of tissue to the electromagnetic field does not cause a temperature rise in local tissue. For mm-sized implants, increasing the operating frequency to hundreds of MHz improves PTE. However, increasing the frequency reduces the maximum allowable power that can be transmitted to the implant due to SAR constraints. The peak SAR limit for RF exposure to a 10-g tissue in the shape of a cube is 10 W/kg in controlled environments [29]. SAR regulation is made for humans, and the use of medical implants was evaluated in [30] and [31] in terms of safety, but it was also used as a reference point in animal research settings to avoid tissue heating due to excess magnetic fields absorbed by animals [13].

3. Design methodology

The use of resonators has already shown improvements in favor of PTE. However, using resonators in the RX side for freely moving rodents in neuroscience applications is not a practical solution. Small mice cannot behave naturally while carrying heavy components. Therefore, the moving part of the inductive link must be kept as small as possible. In an inductive power link, the sizes and shapes of primary (TX) and secondary (RX) coils, and the distance between the two mainly define the PTE of the link. For the neuroscience applications including optical stimulation and neurorecording where power is transferred to a small device attached or implanted into

laboratory mice, size and weight of the RX coil must be chosen carefully. The steps taken in the design of the presented system are shown in the flowchart of Figure 3 and described below.

3.1. Operating frequency

The choice of operating frequency of a WPT system in living tissue should be determined by the SAR, which is dominated by the induced electric field inside the homogeneous tissue and can be calculated as:

$$SAR = \frac{\sigma |\mathbf{E}|^2}{\rho} \quad (2)$$

where σ (S/m) and ρ (kg/m³) are the conductivity and mass density of the exposed tissue, respectively, and \mathbf{E} (V/m) is the root mean square (RMS) electric field strength in tissue [29]. The relation between the frequency of the magnetic field and the SAR is found by solving Maxwell's equation for the electric field, \mathbf{E} [16, 32]:

$$\nabla \times \mathbf{E} = -\frac{\partial \mathbf{B}}{\partial t} \propto f \cdot I_1 \quad (3)$$

where \mathbf{B} is the magnetic field and I_1 is the AC current that the primary coil carries. Therefore, if L_1 carries a signal (I_1) with frequency f , SAR will be proportional to $(f \cdot I_1)^2$ [32]. Thus, if f decreases, I_1 can be increased by the same order, resulting in a significant improvement in the maximum PDL under the SAR limit. However, the frequency should not be decreased to the sub-MHz range, as this could result in tissue heating due to the ohmic losses of the TX coil and power amplifier [16]. On the other hand, a higher operating frequency leads to better PTE and a smaller RX coil, which contrasts to having a safe system. The operating frequency should be within the Industrial, Scientific, and Medical (ISM) frequency bands. Among the two widely used ISM bands (6.78 MHz and 13.56 MHz), we aim for the lower band of ISM, i.e., 6.78 MHz, for the sake of a safer power transfer. According to (2) and (3), for the same amount of input power, the SAR increases by a factor of four when the frequency is raised from 6.78 MHz to 13.56 MHz. It is important to note that further decreasing the operating frequency, reduces the PTE, necessitating a significantly larger RX coil to maintain an acceptable PTE.

3.2. Diameter of the TX based on the distance to the RX

To have a robust inductive link for practical neuroscience applications, the RX coil should be selected as small as possible and the link design should not include a resonator circuit on the RX side for the reasons given previously. Instead, by choosing the right specifications for the TX and RX coils and increasing their SRFs, we can maximize the coupling coefficient, K_{12} which is derived from the mutual inductance between TX and RX coils. The size and weight of the receiver coil is limited by the total load that can be carried by laboratory mice. On the transmitter side, given that a standard homecage area measures 29 cm × 18 cm, an array of TX coils in parallel is ideal. For maximum efficiency between each individual TX coil and the RX coil, it is generally recommended not to use very large coils on the transmitter side. However, the size of each individual TX coil should be designed while considering the following factors:

- (a) A small TX coil has a reduced effective area, necessitating a higher number of coils in the TX array to cover the entire homecage area. Together with the overlapping coils, a significant number of coils are required in the TX array. This adds a considerable amount of parasitic capacitance, resulting in a lower SRF. Consequently, quality factor of the TX array decreases which further reduces the PTE.
- (b) As shown in Figure 4, a smaller TX coil provides a better coupling coefficient, K_{12} , only at shorter distances. For the RX and TX coils shown in Table 1, when TX coil diameter increases from 6.4 cm to 11.2 cm, the reduction in coupling coefficient is almost negligible at 4 cm distance but significant at 1 cm distance.

Therefore, since this work focuses on transferring power over distances greater than 4 cm, the TX design features a larger diameter. This approach considerably reduces K_{12} for short distances, such as 1 cm, but this is not a major concern for this application. Instead, the wide effective area achieved is highly beneficial. The work in [33] also showed that when the distance between TX and RX coil increases, the size of TX should be made larger. There is a relationship between the optimum geometric values of RX outer diameter (dR_{out}), TX outer diameter (dT_{out}), and the distance between the two (d). For a case when $d/dR_{out} = 4$, the optimum ratio of dT_{out}/dR_{out} is around 13 [33].

3.3. Impact of the parasitic components on Q factor and SRF

The values of inductance and parasitic resistance of a coil increase with frequency until they reach their SRF values. Since the parasitic resistance increases at a faster pace than the inductance, the quality factor of the coil,

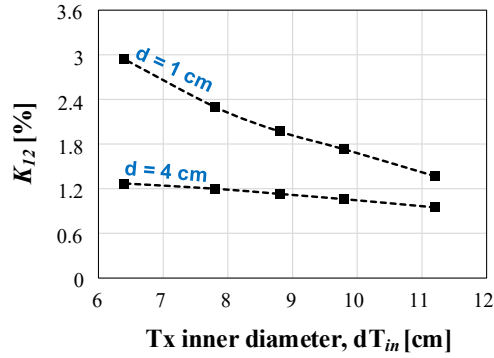


Figure 4. Variations of K_{12} with the TX coil diameter for two distances, 1 and 4 cm.

Table 1. Specifications of TX single coil and RX coil used in HFSS.

| | TX single coil | RX coil |
|----------------------|----------------|--------------|
| Number of turns | 6 | 12 |
| Inner diameter | 11.2 - 13 cm | 7 mm |
| Outer diameter | 15.1 - 17.2 cm | 14 mm |
| Weight | - | 0.17 g |
| Inductance | 10.56 μ H | 1.77 μ H |
| Parasitic resistance | 1.4 ohms | 1.5 ohms |
| Quality factor | 322 | 49 |

$Q = L\omega/R$, reaches its peak at a frequency below the SRF. A good design can be achieved when the peak value of the quality factor occurs at the desired operating frequency, thereby maximizing the coupling coefficient. The shape and material of the coils also impact the coefficient. For example, a circular coil for the receiver (RX) can provide a better quality factor and SRF compared to a rectangular one, as it requires less wire to achieve the same number of turns. However, for the transmitter (TX), since an array of coils is used, employing circular shapes would result in less effective areas at the corners and sides. To ensure the TX is compatible with a circular-shaped RX coil, an octagonal-shaped coil on a printed circuit board (PCB) was used in this work. It is noteworthy that, compared to the PCB-designed coil shown in Figure 6, a wire-wound TX coil with a wire gauge of 12 (approximately 2 mm in diameter) and the same diameter and number of turns does not behave as an inductor at 6.78 MHz. Due to the very large cross-sections between each turn, the accumulated parasitic capacitances increase, and the coil exhibits a very low SRF. For the same diameter and number of turns, the TX coil designed on a PCB offers a higher SRF. The choice of trace thickness, t , depends on the spacing between nearby traces. By increasing t , the Q -factor of a coil appears to increase; however, the parasitic capacitance between nearby traces also increases, which lowers the SRF and consequently reduces the Q -factor. To verify this statement, we calculated parasitic capacitance (C_P) and SRF with different trace thicknesses and showed in Figure 5. First, we obtained inductance at zero frequency (L_{DC}) by simulation for different values of t , then solved for C_P using

$$C_P = \frac{1}{(2\pi \cdot \text{SRF}_0)^2 \cdot L_{DC}} + \epsilon_0 \cdot \frac{t \cdot l}{s} \quad (4)$$

where SRF_0 is the self resonance frequency of the coil at $t = 1$ oz and is obtained by simulation which is around 22.2 MHz, l is the total length of traces that have nearby traces, and s is the spacing between nearby traces. Subsequently, the SRF is calculated using $1/2\pi\sqrt{L_{DC} \cdot C_P}$. In Figure 5, the trace width is 2 mm and s is 1.5 mm, which shows by increasing t from 1 to 32 oz (approximately 1 mm), C_P continues to increase, and therefore, SRF continues to decrease. The coil of Figure 6(a) was used in the calculations above.

3.4. Coil geometry and finite element method solver

We employ the Finite Element Method (FEM) solver to simulate and analyze the electromagnetic behavior of the inductive coupling. To analyze the coefficient between the TX and RX using simulations, a lightweight receiver coil with specifications shown in Table 1 is used. To allow for a maximum PTE, the TX coil is designed based on the RX coil that is forced by the application. The design of a single TX coil, which is given in Table 1, is conducted based on having a small non-effective area. Thus, the traces' width and spacing and the number of

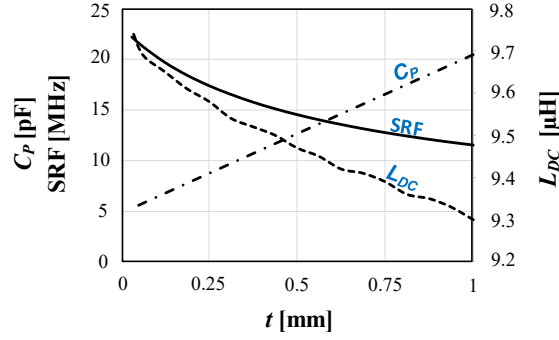


Figure 5. Calculations of C_p , L , and SRF with trace thickness.

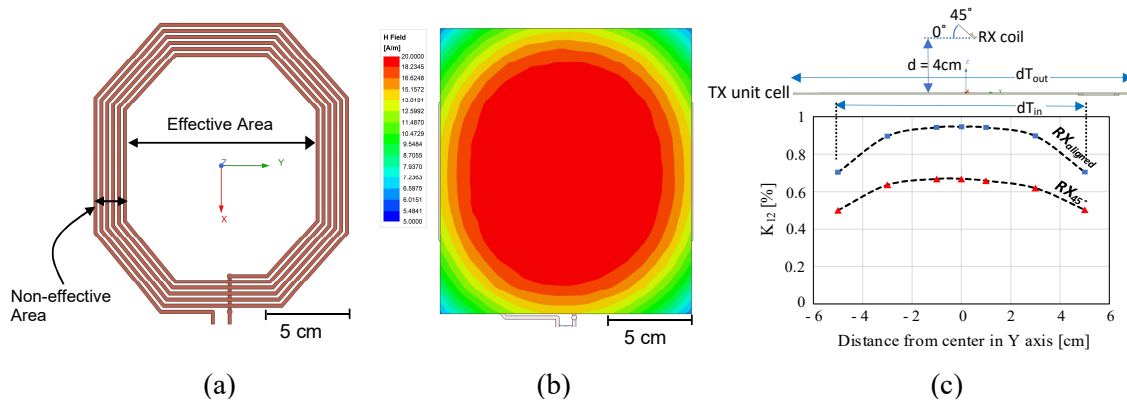


Figure 6. (a) Topology of the TX unit cell, (b) magnetic field distribution at 4 cm above the surface per 1 W of input power and (c) coupling coefficient for the cases of aligned and 45°-misaligned RX coil at 4 cm above the surface (dT_{out} and dT_{in} denote the outer and inner diameters of TX unit cell in y-axis).

turns were reduced to the point where the peak value of quality factor occurs at the operating frequency, 6.78 MHz. This defines the traces' width and number of turns as well. The trace thickness in this design was chosen 2 oz to have a better SRF. At lower heights, the magnetic fields of each trace cancel out the fields of the subsequent trace on the non-effective area of the coil. Given that the height of laboratory mice in walking and rearing positions ranges from 3 cm to 6 cm [34], we have selected a minimum distance of 4 cm as the requirement for this application and conducted the simulation accordingly. The diameter of the spiral TX coil is designed to produce a uniform magnetic field at this height. For an input power of 1 watt in the lumped model, Figure 6(b) shows the distribution of magnetic field strength (\mathbf{H} -field) above the surface of the single coil. It demonstrates that the \mathbf{H} -field at a distance of 4 cm is more than 18 A/m inside the coil's effective area. A critical factor that determines the coupling coefficient between TX and RX coil is alignment. Since in this application the mouse's head undergoes random movements during its natural behavior, the alignment between the TX and RX coils can be disrupted, which may reduce the coupling coefficient. Therefore, we simulated K_{12} between the TX and RX coils for two cases: 0° and 45° misalignment of the RX coil relative to the horizontally placed TX coil. Figure 6(c) shows a reduction of coupling coefficient from 0.95 % to 0.67 %, for the cases of 0° and 45°, respectively. The quality factor as a function of frequency is plotted in Figure 7(a), showing a Q -factor of 320 at 6.78 MHz and an SRF of 22.2 MHz. To obtain the PTE of this two-coil system, (5) can be applied:

$$PTE = |S_{21}|^2 \times 100\% \quad (5)$$

where S_{21} is the transmission coefficient between the TX and RX coils. According to Figure 7(b), S_{21} at the frequency of 6.78 MHz is -6.7 dB, resulting in a maximum PTE of 21% when the distance between TX and RX coils is 4 cm. To cover the entire area of a standard home cage with TX coils, three single coils are employed in parallel, as depicted in Figures 8(a) and (b). The middle coil (L_b) deteriorates the parasitic components of the overall topology; however, the role of L_b is to compensate for the flux that gets cancelled in the middle by the equal fluxes of L_a and L_c . In order to evaluate the impact of adding a third coil (in the middle) on the SRF, the equivalent inductance of L_1 at zero frequency should be calculated. By ignoring the mutual inductance M_{ac} and

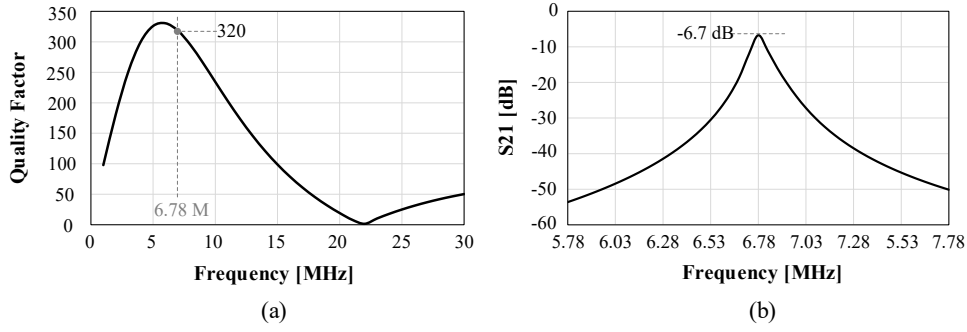


Figure 7. HFSS simulation for (a) Q factor of the TX coil unit cell and (b) transmission coefficient, S21, for the RX coil given in Table 1, at a distance of 4 cm.

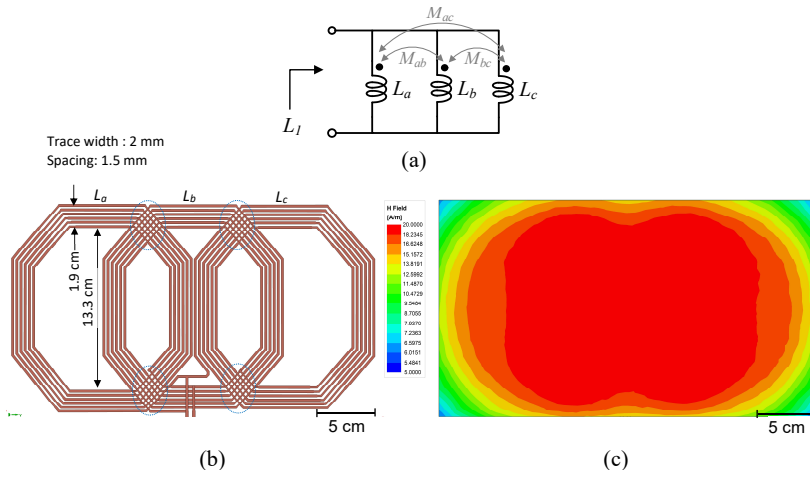


Figure 8. TX three-coil array (a) schematic, (b) overlapping coil array PCB board, and (c) magnetic field distribution at 4 cm above the surface per 1 W of input power.

assuming that M_{ab} and M_{bc} are equal due to symmetry, we have:

$$L_1 = \frac{L_a^2 - 2M_{ab}^2}{3L_a - 4M_{ab}} \quad (6)$$

From (6), it is clear that the value of L_1 is always greater than $1/3 \times L_a$. Besides, since L_b overlaps with both L_a and L_c , the accumulated parasitic capacitances, shown in the four circled areas of Figure 8(b), contribute further to the overall parasitic capacitances. If the parasitic capacitance of each individual TX coil is C_a , then the overall parasitic capacitances of L_1 become significantly greater than $3 \times C_a$. Consequently, having values of $> 1/3 \times L_a$ and $> 3 \times C_a$ in SRF equation, results in a considerable reduction of SRF value for the triple-coil topology. To mitigate this problem, the traces in the overlapping area are narrowed from 2 mm to 1.35 mm, as shown in Figure 8(b). Since the length of the narrowed traces is not too long, it does not have a significant effect on the overall parasitic resistance of L_1 . Overall, there are 144 cross-sections that form the overlapping traces. With a 1-mm thickness of the FR-4 substrate, the reduction of accumulated parasitic capacitance, C_0 , is given by:

$$C_0 = C_{P1} - C_{P2} = \frac{144 \cdot \epsilon_0 \cdot K}{d_{FR4}} \times [(2 \text{ mm})^2 - (1.35 \text{ mm})^2] = 12.3 \text{ pF} \quad (7)$$

where ϵ_0 is 8.85×10^{-12} F/m, K is the relative permittivity of the FR-4 board, 4.4, and d_{FR4} is the thickness of the FR-4 board (1 mm). This results in a significant improvement in the SRF compared to the regular coil design. Using this simple yet effective method, the overall parasitic capacitance, C_P , of L_1 is reduced from 35 pF to 22.7 pF. For the two designs, we have two different SRFs described as follows:

$$\text{SRF}_1 = \frac{1}{2\pi\sqrt{L_{DC} \times C_P}} = 14.4 \text{ MHz} \quad (8)$$

$$\text{SRF}_2 = \frac{1}{2\pi\sqrt{L_{DC} \times (C_P - C_0)}} = 17.8 \text{ MHz} \quad (9)$$

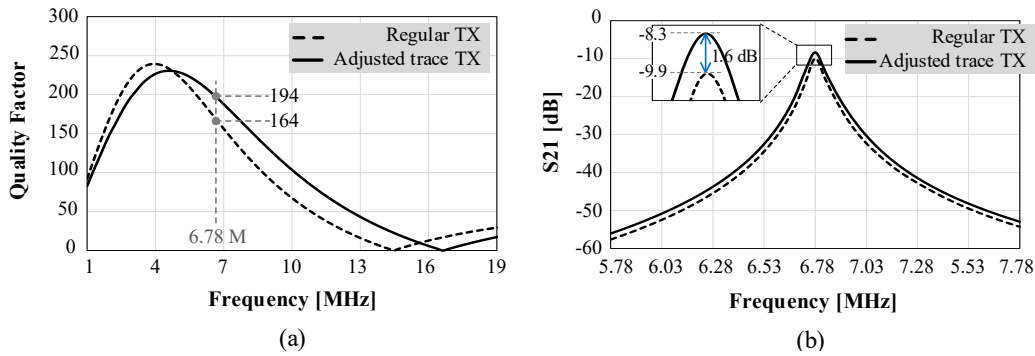


Figure 9. HFSS simulation for the TX coil array for (a) Q factor, showing the peak value of Q and the SRF shifted to a higher frequency and (b) the corresponding S_{21} for the RX coil in Table 1, at 4 cm distance.

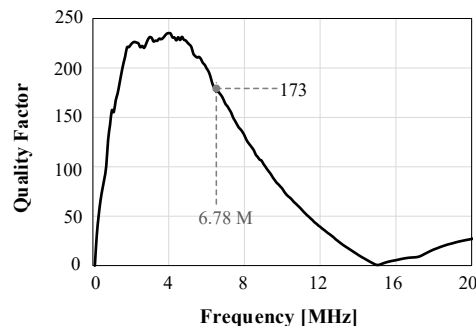


Figure 10. Measurement of Q factor for the optimized TX coil.

where L_{DC} is the inductance of L_1 at zero frequency. According to the calculations in (8) and (9), SRF_2 is 17.8 MHz, which is 3.4 MHz higher than SRF_1 . Simulation of the quality factor for both designs, shown in Figure 9(a), indicates a 2.3 MHz increase in SRF from 14.4 MHz to 16.7 MHz. HFSS simulation demonstrates that reducing the width of overlapping traces significantly shifts the SRF to a higher frequency, resulting in a higher quality factor at 6.78 MHz. As depicted in Figure 9(a), the quality factor increased from 164 to 194, leading to a 1.6 dB increase in S_{21} . Figure 9(b) illustrates S_{21} when the TX coil is set to port 1 and the RX coil to port 2, as a two-coil inductive link. With S_{21} of -9.9 dB, a PTE of 10.2% is achievable, while with S_{21} of -8.3 dB, the PTE would reach 14.8%, indicating a 45% increase. Compared to the single coil in Figure 6, the SRF in the TX coil of Figure 8 decreased from 22.2 MHz to 16.7 MHz, and the frequency at which the peak value of the Q-factor occurs decreased from 6 MHz to 5 MHz. This confirms that the number of parallel coils in the TX array should be minimized to optimize the quality factor.

3.5. SAR evaluation

The safety assessment for living tissue exposed to an electromagnetic field was conducted using Ansys HFSS. In this simulation, the average density of mouse tissue was considered to be 1.065 g/cm^3 [35] with a conductivity of 0.6 S/m. According to regulation [29], the Peak Spatial-Average SAR (psSAR) for 10 g of tissue in the shape of a cube should not exceed 10 W/kg, and the maximum permissible exposure for the general public should be less than 121.5 V/m. Based on simulation in HFSS with an input power of 3 W, the psSAR, according to IEC/IEEE 62704-4 Draft, is 1.75 W/kg and the maximum electric field inside the tissue is 45 V/m at 6.78 MHz. This simulation was performed using a cube with dimensions of $[22 \text{ mm}]^3$, made from a material similar to mouse tissue. The presented method for designing the inductive WPT system for live animal experiments focuses on having a lightweight and compact receiver coil, ensuring minimal interference with the animals' natural behavior. The selection of the operating frequency, TX coil size based on the distance to RX, and minimization of parasitics resulted in a design with high PTE while limiting electromagnetic interaction with tissues by adhering to safety standards.

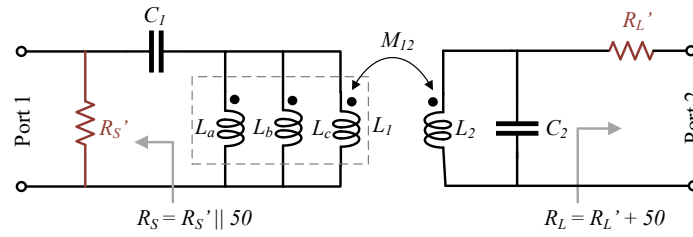




Figure 11. Measurement of actual S_{21} and PTE with the optimum source and load resistor. Port 1 and Port 2 are connected to Ports 1 & 2 of the Network Analyzer, respectively.

Table 2. Specifications of RX₁ and RX₂ coils.

| | RX1  | RX2  |
|---------------------------------|---|---|
| Number of turns | 18 | 10 |
| Inner diameter | 11 mm | 9 mm |
| Outer diameter | 16 mm | 14 mm |
| Weight | 0.4 g | 0.46 g |
| Inductance @ 6.78MHz | 10.67 μ H | 1.5 μ H |
| Parasitic resistance @ 6.78 MHz | 20 ohms | 1.2 ohms |
| Quality factor @ 6.78 MHz | 22 | 52 |

4. Measured performance

The TX coil was fabricated on a two-layer FR4 PCB, and its measured Q factor is shown in Figure 10. The SRF is 15 MHz, with a Q factor of 173 and an inductance value of 4.65 μ H at 6.78 MHz. To measure the PTE of the inductive link, a Network Analyzer E5061B is used, which provided the transmission coefficient (S_{21} parameter) for 50 Ω source and load resistors. However, the optimal values of the source resistor (R_S) and load resistor (R_L) that maximize efficiency may differ from 50 Ω . To measure the actual S_{21} under these optimal R_S and R_L values, additional resistors R'_S and R'_L are used, as shown in Figure 11, where S_{21R} is defined as the actual transmission coefficient [36]:

$$|S_{21R}|^2 = |S_{21}|^2 \times \frac{(R'_S + 50)}{R'_S} \times \frac{(R'_L + 50)}{50} \quad (10)$$

Since the Q factor and SRF of the RX coil also have a significant impact on the PTE of the inductive link, we used two different RX coils with nearly the same weight but different Q factors and measured the PTE separately using the setup shown in Figure 12(a). The Q factor of the two RX coils is measured with frequency and is shown in Figure 12(b). The SRF for RX₁ is at 11 MHz, while for RX₂, it is at 74 MHz. Therefore, the frequency at which the peak value of Q occurs for RX₂ is much higher than that for RX₁. The specifications of the two RX coils are provided in Table 2. The S_{21} and S_{21R} parameters for both RX₁ and RX₂ are shown in Figures 12(c) and (d), respectively. The maximum S_{21R} values for RX₁ and RX₂ are -14.7 dB and -11.2 dB at 6.78 MHz, which correspond to PTEs of 3.3% and 7.5%, respectively. In Figure 13, S_{21R} is measured across a range of R_L values with R_S set to 6.3 Ω . Based on the measurement, the optimal R_L values for RX₁ and RX₂ are 800 Ω and 2 k Ω , respectively. The optimal R_S value during PTE measurement using S_{11} parameter was found to be 6.3 Ω ; however, for PDL measurement, the output resistor of the class-E power amplifier (PA) must be considered, as it will act as the source resistor for the TX coil.

The PDL for both RXs was measured using a Spectrum Analyzer. The class-E PA [37] was powered by a 20 V, 0.3 A source connected to the PCB shown in Figure 14. The entire PCB consumes 6 W, which includes two DC/DC converters, an Xtal oscillator, a gate driver, and the PA. Each of the DC/DC converters have a 90% efficiency. The oscillator and the gate driver consume 27.5 mA and 85 mA, respectively. From the 6 W of power source, these four blocks account for a consumption of more than 2.4 W. Therefore, the PA consumes less than 3.6 W, of which approximately 3 W drives the primary coil of the transmitter, considering the switch loss. To measure the PDL, a series load resistor was added for each measurement to achieve the optimal load values which are 800 Ω for RX₁ and 2 k Ω for RX₂. The maximum unregulated PDL at a single point above the TX coil at a distance of 4 cm for RX₁ and RX₂ is shown in Figures 15(a) and (b), accounting for 21 dBm (126

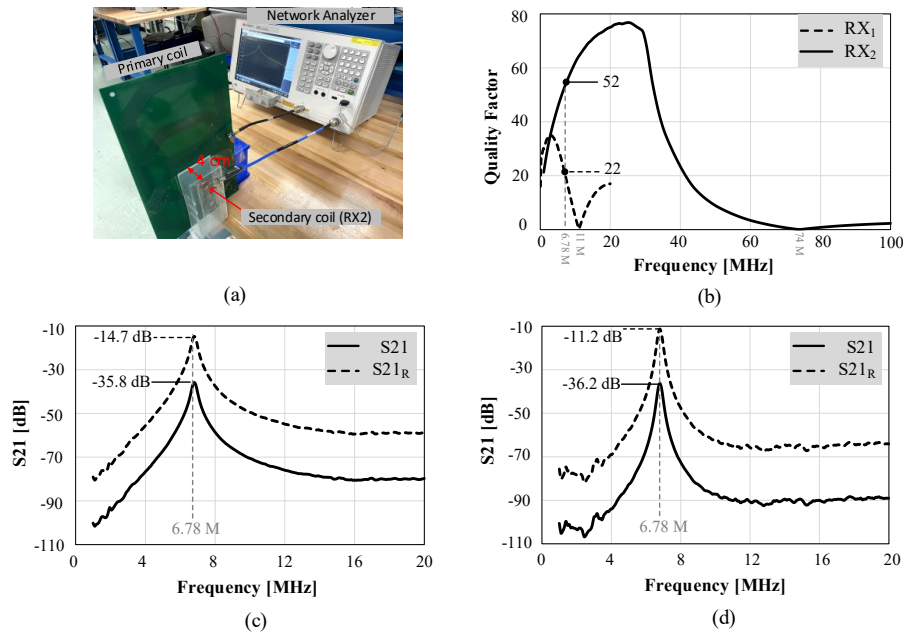


Figure 12. (a) Measurement setup on the Network Analyzer to obtain (b) quality factor of RX_1 and RX_2 , (c) S_{21} for optimal R_S and R_L for RX_1 and (d) S_{21} for optimal R_S and R_L for RX_2 .

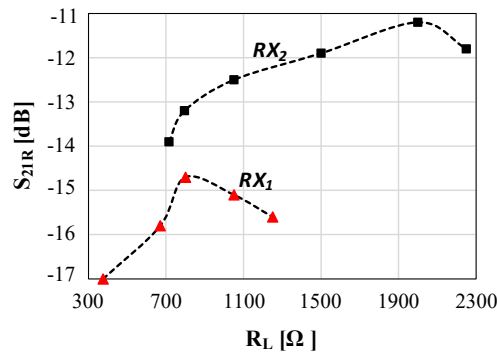


Figure 13. Maximum S_{21R} at the optimal R_L values for both RX_1 and RX_2 coils, when R_S is set to 6.3Ω .

mW) and 23.8 dBm (240 mW), respectively. The points where maximum PDL occur are in the center of the overlapping coils (either $L_a - L_b$ or $L_b - L_c$). Also, the PDL was measured for 98 points and averaged on a surface chart that represents the homepage area. At a 4 cm distance between the transmitter and receiver, RX_1 yields an average unregulated PDL of 73 mW (Figure 15(c)), while RX_2 yields an average unregulated PDL of 127 mW (Figure 15(d)). To evaluate the performance of the WPT system under misalignment, Figures 15(e) and (f) show the average unregulated PDL for RX_1 and RX_2 when there is a 45° -misalignment between receiver and transmitter coils. For the measurement of PDL under misalignment, the angle opening of RX coil was in the same direction for all 98 measured points.

According to the peak spatial-average SAR (psSAR) simulated in Section 3.3, a 3 W power source applied to the TX coil results in a psSAR of 1.75 W/kg for 10 g of tissue at a 5 mm distance between the TX and the tissue sample, which does not exceed the maximum limit of 10 W/kg.

5. In-vivo validation

The WPT system was demonstrated within a realistic experimental *in-vivo* setup involving a laboratory mouse. A complete receiver circuit was designed to receive and regulate power, charge a battery, monitor the received current and battery voltage, and transmit the in-situ measured WPT performance to a base station in real-time via Bluetooth Low Energy (BLE). This WPT system and the receiver circuits powered a wireless electrophysiology

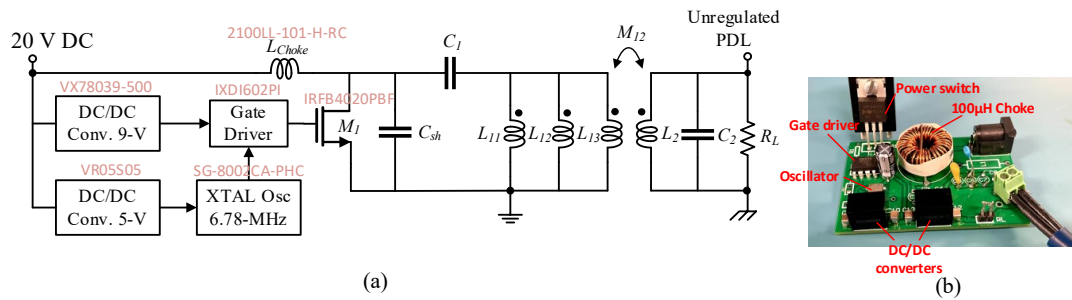


Figure 14. (a) circuit implementation for the measurement of unregulated PDL and (b) class-E PA.

recording headstage [38], which was mounted on the head of the mouse and implanted in the hippocampus. The RX circuit was designed as an adapter between a recording implant and the wireless electrophysiological recording headstage. The headstage is used to monitor neural activity in the brain of the mouse while it freely behaves in its home cage. Figure 16(a) shows the RX circuit, which includes a coil, resonant capacitor, voltage rectifier, Zener diode for protection, a 4.2-V LDO for battery charging, and a Schottky diode with low dropout voltage to protect the battery from feedback current. The headstage, detailed in [38], includes a neural front-end integrated circuit, an MBN52832 BLE wireless transceiver, a 1.8-V LDO, and a tiny LiPo 23-mA battery. A second battery is also packaged on the headstage setup, typically used for optical stimulation, although it was not utilized in the reported experiment. Figure 16(b) shows the power recovery circuit, and Figure 16(c) depicts the entire experimental setup, including the wireless headstage and the RX power and monitoring circuit adapter connected together. Figure 16(d) presents the electrophysiology implant purchased from Doric Lenses, Quebec City, CAN.

To assess the capability of the WPT system to supply the headstage and charge the battery while efficiently recording multi-unit activity in neural tissue in an *in-vivo* setting, an 8-week-old male C57Bl/6J mouse (JAX #000664; Jackson Laboratory) was used. The mouse, weighing between 20 to 27 g, was implanted with a custom fiberless and wireless (Fi-Wi) optoelectric implant from Doric Lenses, Canada. The implant featured an optic fiber (200 μm core, 0.66 NA, 1.6 mm long), three tungsten microelectrodes (75 μm flat tip, 1.8 mm long, with an impedance of 0.5 to 1.2 M Ω), an external silver reference wire, and a Molex connector for headstage connection. Following a small craniotomy over the left hemisphere, a small section of the dura mater was removed to facilitate the insertion of the Fi-Wi optoelectric implant into the left hippocampal CA1 region (R/C -2.20 mm, M/L 1.75 mm, D/V -1.60 mm, insertion speed 160 $\mu\text{m}/\text{min}$). A flat head bone screw was used to anchor dental cement to the skull and support the silver reference wire, enhancing electrode referencing and reducing movement-related artifacts. Dental acrylic (No. 186-1068/4477 and 1119, Henry Schein Ash Arcora) was then used to secure the implant to the skull, ensuring that no wires were exposed. *In-vivo* recordings were conducted at least 4 weeks post-surgery.

The mouse was first anesthetized with less than 4% isoflurane in oxygen to facilitate headstage connection and disconnection. Electrophysiological signals were recorded for a minimum of five minutes while the animal was free to move in a standard plastic cage. The cage has a thickness of around 5 mm, so the animal is protected from direct contact with the transmitter coil. Figure 17 shows the results from the *in-vivo* experiment. The recovered power and battery voltage measured by the adapter while the mouse was freely moving inside the cage, above the transmitter coil array, are shown in Figure 17(a). It indicates that the system, starting with an empty LiPo battery, can be powered by the WPT alone while charging the battery with the recovered power. The variations in charging power are attributed to the movements of the mouse in different directions and the angular movements of its head. On average, the recovered power within the presented 15 minutes of recording was 46 mW, which exceeds the minimal requirement of 32 mW to supply the headstage [38]. Figure 17 shows the neural activity recorded simultaneously, synchronized with the measured charging performance while the mouse roamed inside the home cage above the multicoil charger. In post-processing, neural action potentials (AP) waveforms were isolated from the time series using a non-linear energy operator (NEO), with a fixed threshold applied. Clustering was performed on the detected waveforms using a combination of principal component analysis (PCA) for feature extraction and K-means for clustering. The resulting APs are superimposed on the time series in Figure 17(b) to illustrate the firing pattern. The mouse's movement is represented by zones that correspond to its position within the home cage during the experiment, as identified in Figure 17(f). This representation aids in comparing the movements of the mouse with the firing pattern and the charging power recovered in the cage. These results suggest that the recorded activity is spontaneous, typical of the hippocampal region of the brain. A zoomed-in version of the time series in Figure 17(e) helps illustrate the difference between the APs and the noise floor. The clustered AP shapes are displayed in Figure 17(d), where two distinct AP shapes

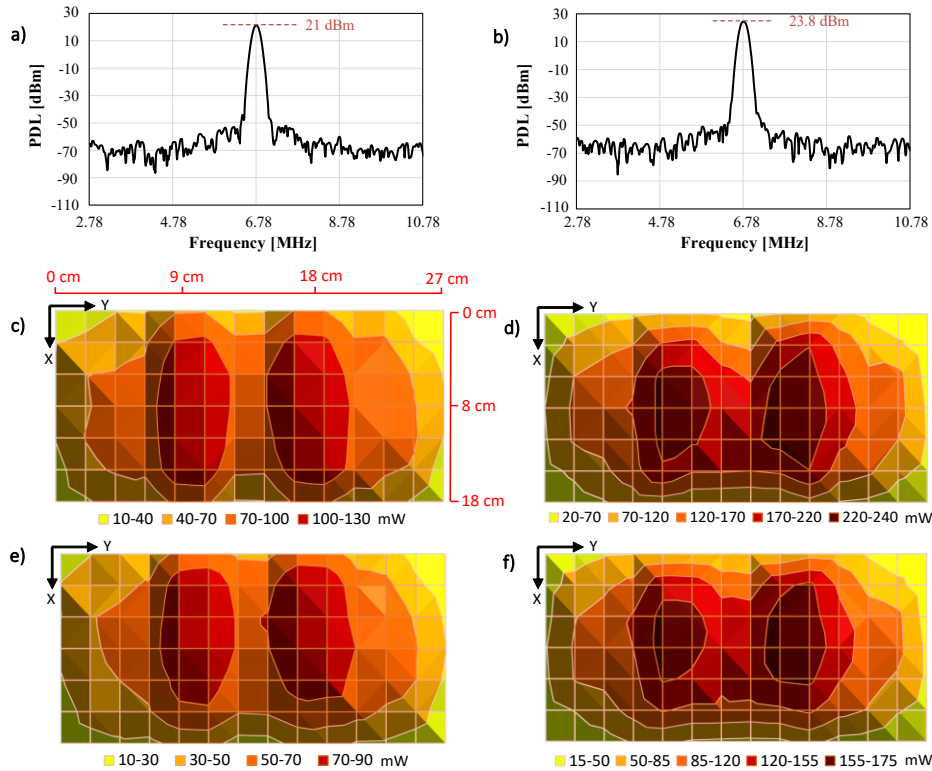


Figure 15. Measurement of maximum and average PDL using Spectrum Analyzer at $d=4$ cm above the surface of TX coil for the area of a standard homecage providing (a) max PDL of 21 dBm (126 mW) using RX_1 , (b) max PDL of 23.8 dBm (240 mW) using RX_2 , (c) average PDL of 73 mW above the surface using RX_1 -aligned, (d) average PDL of 127 mW above the surface using RX_2 -aligned, (e) average PDL of 51 mW above the surface using RX_1 with 45° -misalignment, and (f) average PDL of 89 mW above the surface using RX_2 with 45° -misalignment.

were isolated from the recorded signal. The firing rate for both of these AP shapes is plotted over time in Figure 17(c), synchronized with the neural data, movement, and charging power, highlighting the spontaneous nature of the activity. The firing pattern depicted is calculated by counting the number of APs within 1-second intervals for each identified AP shape. This firing rate is expressed in APs per second using the detected and clustered APs from Figure 17(d). With this proof-of-concept experiment, we demonstrate that the WPT system can recover sufficient power to supply a wireless electrophysiological recording system. Furthermore, the RX circuit is compact and lightweight enough for a mouse to carry in a freely moving setting. A performance comparison of recent works that provided wireless power for neural recording or stimulation during *in-vivo* experiments with mice/rats is presented in Table 3. A single lightweight RX coil with the lowest weight was used in this work which enables the natural and unrestricted movement of the mouse within the homecage.

6. Conclusion

This work presented a design methodology that offers a safe and reliable wireless power transfer system for electrophysiological recording and neural stimulation in freely moving laboratory mice. We demonstrated effective optimization of an inductive link, with a focus on Q factor, SRF, and PDL while keeping SAR under the regulation limit. The presented WPT system includes enhanced specifications of the TX coil through trace adjustments that lead to an improved SRF and higher Q factor. The choice of this topology resulted in eliminating the need for a resonator circuit or additional RX coil. Using a 0.46-g RX coil at 6.78 MHz, the system achieves a maximum PTE of up to 7.5%, and PDL measurements within the homecage indicate an average of 127 mW at a distance of 4 cm, when 3 W of power is driven into the primary coil using a class-E PA. Importantly, the system maintains safety, with psSAR of 1.75 W/kg, which is well below regulatory limits. The design approach prioritized a lightweight and compact receiver coil, minimizing interference with the animals' natural behavior. This, combined with careful optimization of TX coil size, parasitic minimization, and selection of the optimal operating frequency, led to a design that balances high PTE with operational safety. These findings indicate that the system's design effectively balances PTE and operational practicality, providing a

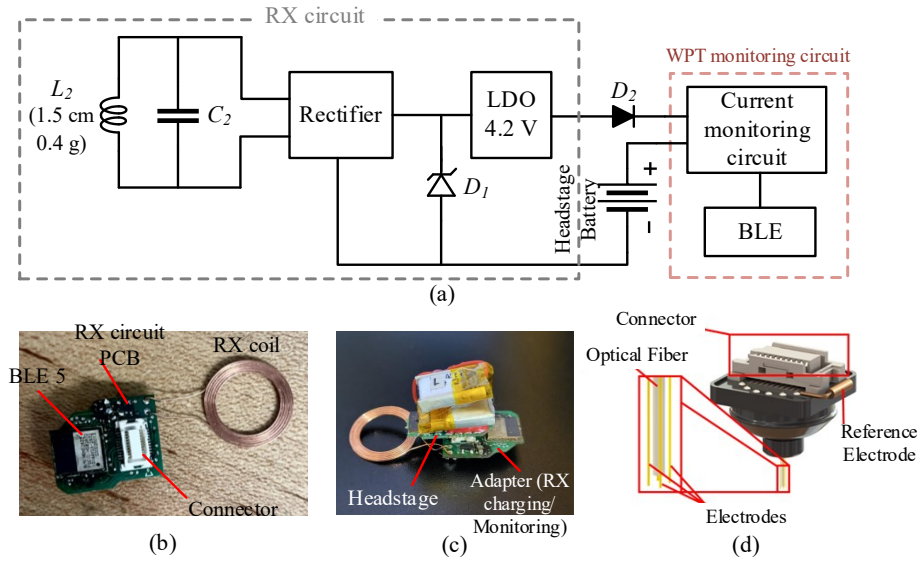


Figure 16. In-vivo measurement setup (a) schematic of the WPT RX circuit that can charge the headstage battery and monitor charging current and battery voltage in real time, (b) RX charging and monitoring circuit designed as a PCB adapter between the implant and the headstage, (c) the headstage and RX circuit connected together, and (d) a photo of the implant manufactured by Doric Lenses, Canada.

Table 3. Comparison with recent works.

| | This work | TBCAS' 23 [25] | TBCAS' 19 [39] | TBCAS' 16 [22] | TBE' 17 [40] |
|---------------------------------|----------------------|----------------------|----------------------|---------------------|----------------------|
| Operating freq. [MHz] | 6.78 | 2.84 | 13.56 | 13.56 | 13.56 |
| Homeage area [cm ²] | 522 | 490 | 1100 | 1100 | 1100 |
| Number of RX coils | 1 | 1 | 2 | 2 | 5 |
| RX coil(s) volume | 0.38 cm ³ | 19.2 cm ³ | 16.2 cm ³ | 2.2 cm ³ | 4.84 cm ³ |
| RX coil(s) weight | 0.46 gram | 6 gram * | > 0.85 gram * | > 0.8 gram * | > 0.9 gram * |
| Max. PTE at d = 4 cm | 14.5 % | 19.6 % | 20.5 % | 18% (avg) | 31.1 % |
| Avg. unregulated PDL @ 4 cm | 127 mW | 0.3-1.93 W @ NA | > 35 mW @ 0-17 cm | 65 mW @ 0-17 cm | > 40 mW @ 8 cm |
| <i>in-vivo</i> experiment with | Mouse | Mouse | Rat | Rat | Rat |

* The weight is estimated based on information given in the paper.

robust platform for real-time neuronal activity monitoring that is verified with continuous *in-vivo* recordings successfully demonstrating the delivery of approximately 46 mW on average to the battery using a lightweight 0.4-g RX coil. The implementation of this high-efficiency power transfer mechanism within a compact and lightweight system paves the way for more extensive and longer-duration experiments, enhancing our ability to study complex neural behaviors in natural settings.

Acknowledgments

We acknowledge the support of the Natural Sciences and Engineering Research Council of Canada (NSERC) [Grant no. RGPIN-2022-03984], the Weston Family Foundation [Grant nos. TR192089 and RR150149], the SMAART Collaborative Research and Training Experience Program (CREATE) funded by NSERC, the Canada First Research Excellence Fund Sentinel North Strategy at Laval University, the Fonds de recherche Québec—Nature et technologie (FRQ-NT) [Grant nos. 2018-PR-207644 and 2021-PR-284207], the Microsystems Strategic Alliance of Quebec funded by FRQ-NT, and the Canada Research Chair in Smart Biomedical Microsystems. We would also like to thank Doric Lenses for manufacturing the implant and providing a picture (Figure 16d).

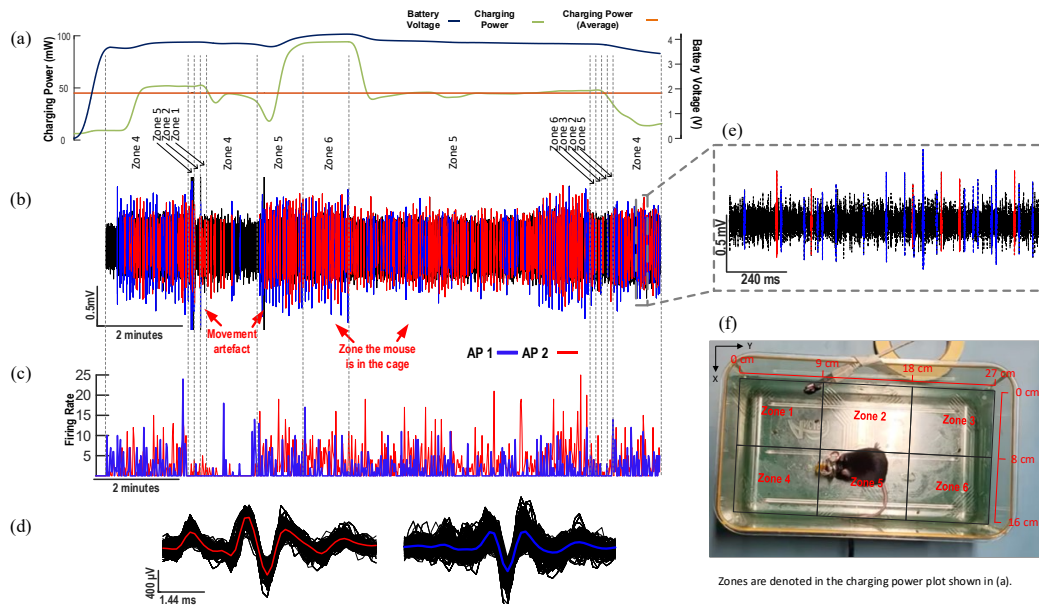


Figure 17. In-vivo measurement results (a) battery voltage, charging power and average power over time for a 15 minute experiment, synchronized with (b) neural data recorded by the wireless headstage with the superimposed detected APs in red and blue and the section of the cage the mouse is in at any given time shown by the numbered zones, (c) the firing rate for both detected APs synchronized with the recordings in (a) and (b) that is calculated by counting the number of APs within 1-second intervals for each identified AP shape, (d) the superimposed clustered AP shapes, (e) a zoomed-in version of the time signal and (f) a photo of the homecage with the mouse location identified as zones during the experiment.

Conflicts of interests

The authors have no conflict of interest.

Authors contributions

Hadi Hayati contributed to the conceptualization, methodology, investigation, visualization, validation, and writing of the original draft, as well as its review and editing. Guillaume Bilodeau supported visualization and validation efforts and provided significant input during the review and editing process. Louison Brochoire provided the resources for the experiment, as well as editing the manuscript. Gabriel Gagnon-Turcotte participated in validation and provided feedback during the review and editing stage. Pascal Fossat contributed to manuscript review and editing. Yves De Koninck provided the resources for the project. Benoit Gosselin supervised the research, managed project administration, secured funding, and contributed to the manuscript's review and editing.

Ethical statement

All experimental procedures were conducted in accordance with guidelines from the Canadian Council on Animal Care and were approved by the committee for animal protection of Université Laval (CPAUL). Approval date: 2022-05-09. Approval number: 2022-1001, VRR-22-1001.

References

- [1] Gagnon-Turcotte G, Bilodeau G, Tsiakaka O, Gosselin B. Smart Autonomous Electro-Optic Platforms Enabling Innovative Brain Therapies. *IEEE Circuits Syst. Mag.* 2020 20(4):28–46.
- [2] Kim CK, Adhikari A, Deisseroth K. Integration of optogenetics with complementary methodologies in systems neuroscience. *Nat Rev Neurosci* 2017 18:222–235.
- [3] Ferenczi E, Deisseroth K. Illuminating next-generation brain therapies. *Nat Neurosci.* 2016 19(3):414–416.
- [4] Borton DA, Yin M, Aceros J, Nurmikko A. An implantable wireless neural interface for recording cortical

- circuit dynamics in moving primates. *J. Neural Eng.* 2013 10(2):1741–2560.
- [5] Yang KW, Oh K, Ha S. Challenges in Scaling Down of Free-Floating Implantable Neural Interfaces to Millimeter Scale. *IEEE Access* 2020 8:133295–133320.
- [6] Das R, Moradi F, Heidari H. Biointegrated and Wirelessly Powered Implantable Brain Devices: A Review. *IEEE Trans. Biomed. Circuits Syst.* 2020 14(2):343–358.
- [7] Jia Y, Khan W, Lee B, Fan B, Madi F, *et al.* Wireless Opto-Electro Neural Interface for Experiments with Small Freely Behaving Animals. *J Neural Eng* 2018 15(4):1741–2552.
- [8] Gagnon-Turcotte G, Keramidis I, Ethier C, Koninck YD, Gosselin B. A Wireless Electro-Optic Headstage With a 0.13- μm CMOS Custom Integrated DWT Neural Signal Decoder for Closed-Loop Optogenetics. *IEEE Trans. Biomed. Circuits Syst.* 2019 13(5):1036–1051.
- [9] Gagnon-Turcotte G, Khirak MN, Ethier C, Koninck YD, Gosselin B. A 0.13- μm CMOS SoC for Simultaneous Multichannel Optogenetics and Neural Recording. *IEEE J. Solid-State Circuits* 2018 53(11):3087–3100.
- [10] Erfani R, Marefat F, Sodagar AM, Mohseni P. Modeling and Experimental Validation of a Capacitive Link for Wireless Power Transfer to Biomedical Implants. *IEEE Trans. Circuits Syst. II: Express Briefs* 2018 65(7):923–927.
- [11] Agarwal K, Jegadeesan R, Guo YX, Thakor NV. Wireless power transfer strategies for implantable bioelectronics. *IEEE Reviews Biomed. Eng.* 2017 10:136–161.
- [12] Mirbozorgi SA, Yeon P, Ghovanloo M. Robust Wireless Power Transmission to mm-Sized Free-Floating Distributed Implants. *IEEE Trans. Biomed. Circuits Syst.* 2017 11(3):692–702.
- [13] Jia Y, *et al.* A Dual-Band Wireless Power Transmission System for Evaluating mm-Sized Implants. *IEEE Trans. Biomed. Circuits Syst.* 2019 13(4):595–607.
- [14] Lee B, Kiani M, Ghovanloo M. A Smart Wirelessly Powered Homecage for Long-Term High-Throughput Behavioral Experiments. *IEEE Sensors J.* 2015 15(9):4905–4916.
- [15] Lee B, *et al.* An Inductively-Powered Wireless Neural Recording and Stimulation System for Freely-Behaving Animals. *IEEE Trans. Biomed. Circuits Syst.* 2019 13(2):413–424.
- [16] Ibrahim A, Kiani M. A Figure-of-Merit for Design and Optimization of Inductive Power Transmission Links for Millimeter-Sized Biomedical Implants. *IEEE Trans. Biomed. Circuits Syst.* 2016 10(6):1100–1110.
- [17] Zargham M, Gulak PG. Maximum Achievable Efficiency in Near-Field Coupled Power-Transfer Systems. *IEEE Trans. Biomed. Circuits Syst.* 2012 6(3):228–245.
- [18] Mirbozorgi SA, Bahrami H, Sawan M, Gosselin B. A Smart Cage With Uniform Wireless Power Distribution in 3D for Enabling Long-Term Experiments With Freely Moving Animals. *IEEE Trans. Biomed. Circuits Syst.* 2015 10(2):424–434.
- [19] Mirbozorgi SA, Jia Y, Zhang P, Ghovanloo M. Toward a High-Throughput Wireless Smart Arena for Behavioral Experiments on Small Animals. *IEEE Trans. Biomed. Eng.* 2020 67(8):2359–2369.
- [20] Zhang P, Jia Y, Mirbozorgi SA, Ghovanloo M. Design of Reactive Resonant Shielding for Multi-EnerCage-HC System. In *IEEE Intl. Symp. Circuits Syst. (ISCAS)*. 2020 .
- [21] Han Y, Zhao L, Jia Y. A Multi-EnerCage-HC System with Reactive Resonant Shielding. In *IEEE Biomed. Circuits Syst. Conf. (BioCAS)*. 2023 pp. 1–4.
- [22] Mirbozorgi SA, Jia Y, Canales D, Ghovanloo M. A Wirelessly-Powered Homecage With Segmented Copper Foils and Closed-Loop Power Control. *IEEE Trans. Biomed. Circuits Syst.* 2016 10(5):979–989.
- [23] Seo DW. Comparative Analysis of Two- and Three-Coil WPT Systems Based on Transmission Efficiency. *IEEE Access* 2019 7:151962–151970.
- [24] Jow UM, *et al.* EnerCage: A Smart Experimental Arena With Scalable Architecture for Behavioral Experiments. *IEEE Trans. Biomed. Eng.* 2014 61(1):139–148.
- [25] Kim J, *et al.* Cage-Embedded Crown-Type Dual Coil Wireless Power Transfer Based Microwave Brain Stimulation System for Untethered and Moving Mice. *IEEE Trans. Biomed. Circuits Syst.* 2023 17(2):362–374.
- [26] Baker MW, Sarpeshkar R. Feedback analysis and design of RF power links for low-power bionic systems. *IEEE Trans. Biomed. Circuits Syst.* 2007 1(1):28–38.
- [27] Kiani M, Jow UM, Ghovanloo M. Design and Optimization of a 3-Coil Inductive Link for Efficient Wireless Power Transmission. *IEEE Trans. Biomed. Circuits Syst.* 2011 5(6):579–591.
- [28] Bilodeau G, *et al.* A wireless electro-optic platform for multimodal electrophysiology and optogenetics in freely moving rodents. *Front. Neurosci.* 2021 15:1–15.
- [29] IEEE standard for safety levels with respect to human exposure to radio frequency electromagnetic fields, 3 KHz to 300 GHz, 2005.
- [30] Shah IA, Basir A, Cho Y, Yoo H. Safety Analysis of Medical Implants in the Human Head Exposed to a Wireless Power Transfer System. *IEEE Trans. Electromagnetic Compatibility* 2022 64(3):640–649.
- [31] Lazzi G. Thermal effects of bioimplants. *IEEE Engineering in Medicine and Biology Magazine* 2005 24(5):75–81.

- [32] Christ A, *et al.* Assessing Human Exposure to Electromagnetic Fields From Wireless Power Transmission Systems. *Proc. IEEE* 2013 101(6):1482 – 1493.
- [33] Harrison RR. Designing Efficient Inductive Power Links for Implantable Devices. *IEEE Int. Symp. Circuits Syst. (ISCAS)* 2007 pp. 2080–2083.
- [34] Burton A, *et al.* Wireless, battery-free subdermally implantable photometry systems for chronic recording of neural dynamics. *Proc. Natl. Acad. Sci (PNAS)* 2020 117(6):2835–2845.
- [35] Boutaleb S. Impact of mouse model on preclinical dosimetry in targeted radionuclide therapy. *Proc. IEEE* 2009 97(12):2076–2085.
- [36] Mirbozorgi SA, Jia Y, Ghovanloo M. Power Efficiency and Power Delivery Measurement in Inductive Links with Arbitrary Source and Load Impedance Values. In *IEEE Life Sci. Conf. (LSC)*. 2018 .
- [37] Sokal NO, Sokal AD. Class E-A New Class of High-Efficiency Tuned Single-Ended Switching Power Amplifiers. *IEEE J. Solid-State Circuits* 1975 10(3):168–176.
- [38] Gagnon-Turcotte G, Keramidis I, Koninck YD, Gosselin B. An Adaptive and Autonomous System-On-Chip with Data Analysis for μ s-Latency Closed-Loop Optogenetics. In *IEEE Biomed. Circuits Syst. Conf. (BioCAS)*. 2023 .
- [39] Lee B, *et al.* An Inductively-Powered Wireless Neural Recording and Stimulation System for Freely-Behaving Animals. *IEEE Trans. Biomed. Circuits Syst.* 2019 13(2):413–424.
- [40] Jia Y, *et al.* Position and Orientation Insensitive Wireless Power Transmission for EnerCage-Homecage System. *IEEE Trans. Biomed. Eng.* 2017 64(10):2439–2449.